To appear in *Molecular Simulation*
Vol. 00, No. 00, Month 20XX, 1–14

ARTICLE

Domain decomposition of the two-temperature model in DL_POLY_4

Michael A. Seaton[a*], Ilian T. Todorov[a], Szymon L. Daraszewicz[b], Galvin S. Khara[b] and Dorothy M. Duffy[b]

[a]*STFC Daresbury Laboratory, Sci-Tech Daresbury, Keckwick Lane, Daresbury, Warrington, WA4 4AD, UK;* [b]*London Centre for Nanotechnology, Department of Physics and Astronomy, University College London, Gower Street, London, WC1E 6BT, United Kingdom*

(*Received 00 Month 20XX; final version received 00 Month 20XX*)

Including the effects of excited electrons in classical simulations, at the level of the two-temperature model, involves the coupling of a grid-based finite-difference solver for a heat diffusion equation and classical molecular dynamics simulations with an inhomogeneous thermostat. Simulation of large systems requires domain decomposition of both particle-based and grid-based techniques. Starting with the CCP5 flagship code DL_POLY_4 as the domain-decomposed molecular dynamics code, we devised a method to divide up temperature grids among processor cores in a similar fashion, including the appropriate communications between cores to deal with boundaries between grid divisions. This article outlines how the domain decomposition of the temperature grids was achieved and gives some example applications of the two-temperature model implementation in DL_POLY_4.

Keywords: DL_POLY, domain decomposition, molecular dynamics, two-temperature model, finite difference method

1. Introduction

The effect of radiation damage on initially well-ordered materials has frequently been studied using cascade simulations (e.g. [1, 2]). Such simulations account for the elastic interactions between the atoms of a material but they often neglect the effects of inelastic scattering where the atoms lose energy by exciting the electrons, commonly referred to as electronic stopping. Electronic stopping can be included in cascade simulations by introducing a friction term in the equation of motion for atoms with energies higher than a specified cutoff; however, this methodology does not account for the energy storage and redistribution of electrons, nor the resulting effects on atomistic dynamics [3, 4]. The redistribution can be achieved by applying a stochastic force [5] with a mean value related to the local electronic temperature. The coupled two-temperature model (TTM)/molecular dynamics (MD) methodology [6, 7] (known as 2T-MD) uses the heat diffusion equation solved on a regular grid of voxels using e.g. the finite difference method (FDM) to evolve the electronic temperature. The energy loss due to electronic stopping and the energy gain due to electron-phonon coupling are added as source and sink terms to the heat diffusion equation during each molecular dynamics step.

Higher energy impacts and depositions require the simulation of structured materials with larger numbers of atoms. Domain decomposition is an appropriate parallelisation strategy for such calculations [8] and several classical molecular dynamics codes make use of it, including DL_POLY_4, the successor to DL_POLY_3 [9, 10] and the code used in this work. Preservation of the high scalability of DL_POLY_4 implies that a parallel implementation of the two-temperature model should also be

*Corresponding author. Email: michael.seaton@stfc.ac.uk

based on domain decomposition by dividing up the electronic temperature grid among processor cores and locally applying the heat diffusion equation to those sections of the grid. The alternative of replicated data – in this case, holding the same temperature grid data on all processor cores – has previously been implemented in LAMMPS [11], but this strategy requires significant MPI communication to gather together and broadcast temperature grid data as well as carrying out FDM calculations over the entire grid on all processor cores. By dividing out the grid over the processor cores and using core-to-core communications, the time spent on evolving the electronic temperature grid will be reduced significantly for larger systems running on thousands of processor cores.

The objective of this work was to implement two-temperature models in DL_POLY_4 for large-scale simulations associated with highly excited electrons – radiation damage cascades and irradiation depositions from lasers and swift heavy ions – with the intention of including this feature in future releases of the code. This article discusses the implications of domain decomposition of grid-based FDM calculations in conjunction with a domain-decomposed MD code, including the necessary strategies for division of temperature grids among cores and inter-core communications for grid boundary voxels. Some applications making use of this new functionality will also be highlighted.

2. Theoretical background and computational challenges

2.1. *Two-temperature model*

The system consists of heavy atoms exchanging energy with a sea of light electrons. The molecular dynamic equation of motion takes the form of a Langevin equation:

$$m_i \frac{\partial \vec{v}_i}{\partial t} = \vec{F}_i(t) - \chi_i m_i \vec{v}_i + \tilde{F}(t) \tag{1}$$

with m_i and $\vec{v}_i$ as the mass and velocity of atom i, $\vec{F}_i(t)$ the force acting on atom i at time t due to interactions with surrounding atoms. Energy loss is included as a friction term with an inhomogeneous coefficient χ_i, whose value for a particular atom depends upon its speed relative to an electronic stopping threshold value v_0 and provides contributions for electron-phonon (χ_p) and electron stopping (χ_s) effects:

$$\chi_i = \begin{cases} \chi_p + \chi_s & |v_i| > v_0 \\ \chi_p & |v_i| \leq v_0. \end{cases} \tag{2}$$

Energy gains from electron-ion interactions can be represented as a stochastic force term $\tilde{F}(t)$ with random magnitude and direction, satisfying the following properties:

$$\begin{aligned} \left\langle \tilde{F}(t) \right\rangle &= 0 \\ \left\langle \tilde{F}(t') \cdot \tilde{F}(t) \right\rangle &= 2 k_B T_e m_i \chi_p \delta(t' - t) \end{aligned} \tag{3}$$

where k_B is the Boltzmann constant and T_e is the electronic temperature. The magnitude of the random force should use the electronic temperature for the grid voxel in which each individual atom is positioned.

The temperature of an electron gas is assumed to evolve by means of a continuum heat diffusion

equation:

$$C_e \frac{\partial T_e}{\partial t} = \nabla \left(\kappa_e \nabla T_e \right) - g_p \left(T_e - T_a \right) + g_s T'_a \tag{4}$$

where C_e and κ_e are respectively the electronic volumetric heat and conductivity, T_a is the local atomic temperature and T'_a is a similar parameter to T_a but only includes atoms with speeds greater than v_0. Both T_a and T'_a are determined for each electronic grid voxel from the average kinetic energy of the atoms contained therein, using peculiar particle velocities to remove any local centre-of-mass drift due to flow effects, i.e. for cell J:

$$\vec{v}_{p,J} = \frac{\sum_{i \in J} m_i \vec{v}_i}{\sum_{i \in J} m_i} \tag{5}$$

$$T_{a,J} = \frac{\sum_{i \in J} m_i \left(v_i - v_{p,J} \right)^2}{3 k_B N_J} \tag{6}$$

$$T'_{a,J} = \frac{\sum_{i' \in J} m_i \left(v_i - v_{p,J} \right)^2}{3 k_B N'_J} \tag{7}$$

The second term in Equation (4) represents energy exchange by means of electron-ion interactions with the relevant coupling coefficient equal to

$$g_p = \frac{3 N_J k_B \chi_p}{\Delta V} \tag{8}$$

where ΔV and N_J are respectively the voxel volume (assumed constant) and the number of atoms inside voxel J. The third term in the heat diffusion equation accounts for energy exchange by electronic stopping and its coupling coefficient is equal to

$$g_s = \frac{3 N'_J k_B \chi_s}{\Delta V} \tag{9}$$

where N'_J is the number of atoms in voxel J subject to electronic stopping (i.e. where $v_i > v_0$).

Equation (4) can be solved numerically using the finite-difference method (FDM), taking the centre of each voxel as its grid point. For this particular application, Euler's method to solve the partial differential equation explicitly is applied, using a forward-difference time derivative and central-difference spatial derivatives based on grid spacings (Δx, Δy, Δz) and timestep (δt). This scheme is illustrated for a one dimension (x) in Figure 1: the temperature at voxel i and timestep $n+1$ (T_i^{n+1}) depends on the same voxel's value for the previous timestep n as well as its nearest neighbours (voxels $i-1$ and $i+1$).

To ensure the explicit form of FDM gives numerically stable solutions, the condition $0 < \frac{\kappa_e \delta t}{C_e (\Delta x)^2} \leq \frac{1}{2}$ would need to be satisfied for a one-dimensional system [12]. Expanding to three dimensions, the following condition would need to be satisfied to obtain stable solutions:

$$0 < \frac{\kappa_e \delta t}{C_e \left(\min \left(\Delta x, \Delta y, \Delta z \right) \right)^2} \leq \frac{1}{6}.$$

This can be obtained by splitting the MD timestep (Δt) into an integer number of divisions, i.e. $\Delta t = N_t \delta t$.

The electronic temperature grid can extend beyond the size of the MD simulation cell to ensure electronic energy is transported away from the atomistic system using appropriate boundary conditions [7]. It is therefore convenient to define a separate ionic temperature grid with a total volume

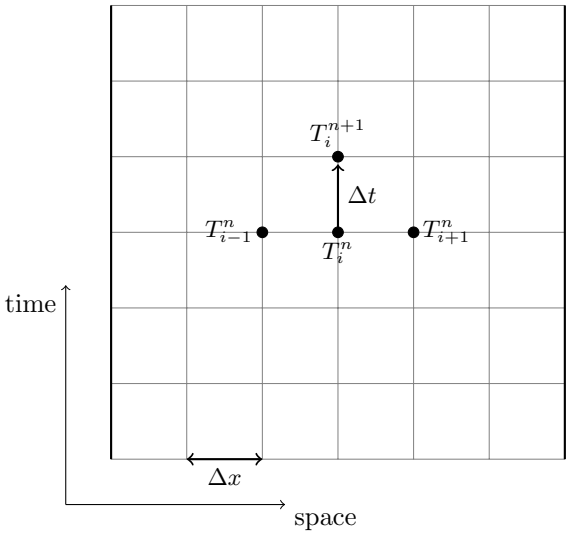

Figure 1.: One-dimensional finite-difference schematic: algorithm is constrained to forward-in-time movement but varies in both spatial directions, with dark vertical lines at the edges indicating boundary nodes.

equal to that of the MD cell; this consists of voxels of equal volume (ΔV) to those in the electronic temperature grid, which are placed in the same locations as electronic temperature voxels *within the MD cell volume*. The heat diffusion equation for electronic temperature grid points outside of the MD cell is evaluated without the two source terms.

Various simulations are available that involve the two-temperature model with MD (2T-MD). Three particular setups include those for radiation cascades and irradiation caused by lasers and swift heavy ions. Cascades make use of electronic temperature grids that extend beyond the MD cell, often using boundary conditions at the edges that remove at least some of the electronic energy from the system: rather than depositing energy into the electronic system at the start of the simulation, one particular atom is assigned a high velocity to inject energy into the entire system. Laser irradiated systems frequently employ pulsed energy depositions that are homogeneous in two dimensions and electronic temperature grids of a similar size to ionic grids with heat conducting boundaries to account for heat and pressure transmission into the bulk film. Swift heavy ion irradiated systems apply energy depositions that vary radially in two-dimensions from a central point and decay exponentially in time: the electronic temperature grid in these systems typically extends far from the MD cell in these two dimensions with energy-removing boundaries as well as closed or periodic boundaries in the third dimension. A fuller description of the use of 2T-MD (molecular dynamics with TTM) is given in [13].

2.2. *Computational issues to address*

Implementing TTM outlined above into the domain-decomposed MD code DL_POLY_4 involves a number of computational challenges:

(1) Divisions of the electronic and ionic temperature grids among processor cores;
(2) Matching up electronic and ionic temperature grids within the MD cell;
(3) Communication of electronic temperatures to neighbouring processor cores to generate boundary halos;
(4) Communication of data to construct ionic temperature grids and calculate source terms.

Since the MD simulation cell is domain decomposed, a similar strategy can be applied for the temperature grids. There is, however, the need to ensure that the ionic and electronic temperatures for a particular voxel can both be found in the same processor core for heat diffusion calculations. Since the evolution of electronic heat diffusion is calculated on a regular grid, any communications between values on a grid should be as efficient as possible to minimise the impact on parallel scalability of the MD code.

3. Implementation

3.1. *Division of ionic temperature grid*

Given that the MD simulation cell is domain decomposed according to its volume, the ionic temperature grid should be divided among processor cores in a similar fashion. To deal with any voxel divided among neighbouring cores, the core with the lowest number in a particular dimension will hold it for the purposes of heat diffusion calculations; e.g. 9 cells would be divided among two cores in the x-dimension by giving the first core 5 cells and the second 4. Additional voxels are also included for each core in all three dimensions to act as a single-voxel boundary halo around the assigned ionic temperature grid cells. The ionic temperature grids are represented in DL_POLY_4 as one-dimensional arrays with the single array index used to identify the Cartesian coordinate of a voxel. Setting N_x, N_y and N_z as the numbers of voxels in each dimension for the given processor core (excluding the boundary halo), the voxel index can be calculated as $N_{i,j,k} = 1 + i + (N_x + 2)(j + (N_y + 2)k)$ for $0 \leq i \leq N_x + 1$, $0 \leq j \leq N_y + 1$ and $0 \leq k \leq N_z + 1$.

3.2. *Division of electronic temperature grid and matching up with ionic temperature grid*

It is assumed that the ionic temperature grid is placed exactly in the centre of the electronic temperature grid with the same number of grid voxels on both sides of the MD cell for each dimension. To match up the electronic and ionic temperature grids inside the MD simulation cell, the electronic temperature grid can be considered as multiples of the entire ionic temperature grid. An equal number of 'unit grids' are assigned on either side of the ionic temperature grid for each dimension. The centre unit grid for electronic temperature is located in the same place as the ionic temperature grid and the two temperature grids are thus matched up precisely.

All unit grids for electronic temperature are divided among processor cores in an identical manner to the ionic temperature grid, including boundary halo voxels. An illustration of the assignment of electronic temperature grid voxels to processor cores can be found in Figure 2. If the number of unit grids required on each side of the central unit grid is not an integer, the next highest integer is selected; provided the boundaries of the entire electronic temperature grid are correctly located and applied in the furthest unit cells, the FDM heat diffusion calculations can be carried out on superfluous electronic temperature voxels without affecting the results. The arrays for electronic temperature grids are represented in DL_POLY_4 as four-dimensional arrays: the first dimension gives the location in each unit grid (in a similar fashion to the ionic temperature grid) while the last three identify the unit grid relative to the centre.

3.3. *Grid temperature communications*

The use of regular grids for electronic and ionic temperatures makes it possible to predict the amount and selection of data to send between processor cores. MPI derived data types can be created to automatically select the grid values to send and receive for each dimension, allowing the use of a single set of MPI send and receive calls (either blocked or unblocked) to send grid values

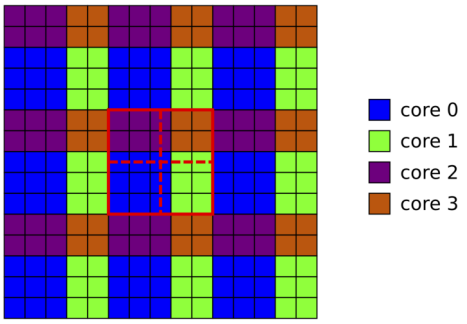

Figure 2.: Illustration of domain decomposition of temperature grids: ionic temperature grid 5×5 voxels, electronic temperature grid 15×15 voxels, four processor cores. Assignment of voxels to processor cores indicated by colour, solid red lines indicate extent of ionic temperature grid and MD cell, dashed red lines indicate boundaries between cores for MD domain decomposition.

for each direction ($\pm x$, $\pm y$, $\pm z$). This is the same communication technique used in DL_MESO for its Lattice Boltzmann Equation code [14] and has been shown to give near-perfect parallel scaling to thousands of cores.

Two sets of derived data types are constructed. One set of data types is made up of double-precision reals for sending electronic temperature values, indicators for active ionic temperature cells (to indicate which cells to ignore when they are devoid of atoms), sums of masses, momenta and kinetic energies for calculations of ionic temperatures and heat diffusion source terms. The other set is made up of integers for atom counters required for ionic temperature calculations. The datatypes are constructed with appropriate choices of blocklength and slide for boundary halos to ensure voxels at sub-grid edges and corners are dealt with correctly when electronic temperatures are sent in the order $+x$, $-x$, $+y$, $-y$, $+z$ and $-z$. These communications are required both within and between the electronic temperature unit grids, the latter of which are dealt with by processor cores at the edges of the MD cell for each dimension. Since the temperature voxels are preferentially given to lower numbered processor cores in each dimension, communications needed to calculate ion temperatures and source terms correctly only need to sent in $-z$, $-y$ and $-x$ directions to reach all ion temperature voxels undergoing FDM calculations.

3.4. *TTM functionalities applied in* DL_POLY_4

While the above describes the essential implementation of the two-temperature model in DL_POLY_4, several options have been included to allow for a wide range of 2T-MD simulations to be carried out.

The inhomogeneous Langevin thermostat with dual friction terms can be activated without making use of the ionic and electronic temperature grids, using the user-specified system temperature instead of the local electronic temperature in Equation (3) for stochastic forces. The removal of electronic stopping energy from atoms still takes place in this case, but this energy is neither stored in electrons nor can it be transferred back to the atomistic system. As such, the inhomogeneous Langevin thermostat alone can be used in cascade simulations to give extremes in initial radiation damage.

When the full TTM is applied along with the inhomogeneous Langevin thermostat, by default the latter is only applied to the thermal component of particle velocities, i.e. the total particle velocities minus the local voxel's peculiar value as determined by Equation (5). Options have been included to apply the Langevin thermostat to total particle velocities, either in all three dimensions

or to x- and y-components (using the z-component of thermal particle velocities in the latter case).

The volumetric heat capacity used in Equation (4) can be specified in one of four ways: (1) a constant value independent of electronic temperature, (2) a linear function of temperature up to the Fermi temperature and a constant (maximum) value beyond it, (3) a hyperbolic tangent function of temperature, or (4) a tabulated function of electronic temperature in a file supplied by the user. In cases 1, 2 and 3, the user can supply parameters for the specific heat capacity: the product of specific heat capacity with atomic density gives the volumetric value. The atomic density is assumed to be constant throughout the system and can either be calculated based on the initial configuration, specified by the user or calculated dynamically based on the number of active ionic temperature voxels.

For metallic systems, the thermal conductivity also needs to be supplied and this can be chosen to be one of four options: (1) infinitely large (i.e. instantaneous heat transfer across the system), (2) a constant value independent of electronic temperature, (3) a linear function of temperature compared to a datum value based on the Drude model, or (4) a tabulated function of electronic temperature in a user-supplied file. Non-metallic systems normally make use of thermal diffusivities (ratios of thermal conductivity to volumetric heat capacity) and these can be specified in one of three ways: (1) a constant value independent of electronic temperature, (2) a reciprocal function of temperature up to the Fermi temperature and a constant (minimum) value beyond it, or (3) a tabulated function of electronic temperature in a user-supplied file.

The electron-phonon coupling friction term χ_p can either be held as a constant value or be dynamically varied according to electronic temperature, using values of g_p given as a tabulated function supplied by the user and Equation (8). When g_p is supplied as a tabulated function, it can either be applied homogeneously across the entire system using a mean electronic temperature or calculated for each voxel using the local electronic temperature.

Various boundary conditions can be applied to the outer edges of the electronic temperature grid: these are not directly connected to any boundary conditions applied for the atomistic (MD) system. The various categories of available boundary conditions include:

- Periodic;
- Dirichlet (infinite flux);
- Neumann (zero flux);
- Robin (partial/variable flux).

Dirichlet boundary conditions fix the temperature at the edges of the electronic grid to a constant value, in this case the target (system) temperature T_0. Neumann boundary conditions set the temperature gradient at the electronic grid edges to zero (i.e. $\frac{dT}{dx} = 0$) by setting the temperature in those voxels to the values of their nearest neighbours. Robin boundary conditions are a hybrid of Dirichlet and Neumann conditions, which set the temperature of the boundary voxels to a fixed proportion between T_0 and the neighbouring voxel's temperature, giving the temperature gradient as $\frac{dT}{dx} = -k(T - T_0)$ where k is the 'target' proportion. All four types of boundary condition can be applied to all six boundaries ($\pm x$, $\pm y$, $\pm z$), or Neumann boundaries in the z-direction can be combined with Dirichlet or Robin boundaries in the x- and y-directions.

For laser excitation and swift heavy ion systems, energy can be deposited to the electronic temperature grid at its centre. The energy deposition can be expressed as a product of spatial and temporal functions. The spatial deposition function can be a constant (homogeneous) value in all three directions, a Gaussian distribution in x- and y- directions (constant in the z-direction), or a homogeneous value in x- and y-directions with exponential decay in the z-direction from the system centre (as used for lasers). The temporal deposition function can be a Dirac delta function (approximated by applying all the energy in a single diffusion timestep δt), a square pulse, Gaussian or exponential functions in time. The user can specify the electron stopping power of a projectile entering the electronic system or the absorbed fluence and penetration depth of a laser, as well as spatial and/or temporal distribution coefficients. In all cases, since the product of the voxel

volume and the integral of the volumetric heat capacity C_e between two temperatures represents a change in electronic energy, the effect of energy deposition can be realised by increasing the electronic temperature of a voxel. That temperature can either be found analytically – if the heat capacity is constant or a known function of temperature – or determined iteratively if tabulated heat capacities are supplied.

A minimum number of atoms are required in each temperature voxel to ensure the ionic temperature is calculated correctly from atom velocities. The absolute minimum number is naturally 1, but the user can specify the minimum number of atoms required in each ionic temperature voxel to consider it active and used in thermal diffusion calculations. If a given ionic temperature voxel becomes inactive, an option exists to transfer the energy from the associated electronic temperature cell to its active neighbours and thus ensure system-wide conservation.

Two options can also be invoked to help initialise systems requiring TTM. One option is to delay the start of an energy deposition (usually applied at the start of a 2T-MD simulation) by a user-specified time, providing time for the atomistic system to settle and equilibrate. The other is to apply electron-phonon coupling in a single direction (from the electronic system to the atomistic system) in Equation (4), i.e. applying the term with g_p only when $T_e > T_a$.

All of the above features have been implemented in the next version of DL_POLY_4 (4.09), which is due for imminent release at the time of writing (February 2018). A further additional functionality to be added later will be atomistic interaction potentials that depend upon electronic temperature. Proposed forms of T_e-dependent potentials include analytical functions with virial terms expanding on electronic temperature [15] and sets of potentials (described either by parameters or in tabulated form) at various electronic temperatures, using interpolation to obtain the potential for a given voxel's temperature [16].

4. Performance of parallelised TTM

As a guide to how well the two-temperature model implementation works in DL_POLY_4, strong scalability tests based on radiation damage cascades [17] have been carried out on Phase 2 of the UK's national supercomputer ARCHER (www.archer.ac.uk). A system consisting of 1 458 000 α-iron atoms in a cubic box with sides of 249.14Å interacting with a tabulated embedded atom model (M07 in [18]) was simulated using between 12 and 1536 processor cores of ARCHER. Two sets of calculations on varying numbers of processor cores were carried out, one using TTM and the other solely using the inhomogeneous Langevin thermostat. The simulations with TTM were carried out on ionic temperature grids of $18 \times 18 \times 18$ voxels (averaging 250 atoms per voxel) inside electronic temperature grids of $54 \times 54 \times 54$ voxels with Robin boundary conditions at the edges, using thermal conductivities given as a linear (Drude-like) function of temperature and tabulated specific heat capacities. In both sets of simulations, the electron-phonon and electronic stopping friction terms for the Langevin thermostat are set as constant values (independent of electronic temperature). The MD timestep size was allowed to vary during the simulations in response to the dynamics of the atomistic system.

An impact of 10 keV was applied to one of the iron atoms to initiate a radiation damage cascade. No energy depositions were made directly to the electronic system in the simulations with TTM, which meant that the electronic heat diffusion calculations (Equation (4)) did not have to be finely subdivided per MD timestep at the start of the calculations. Between two and four electronic temperature evolutions per MD timestep were required for 2T-MD simulations, depending on the timestep size.

The timings of the calculations are shown in Table 1 and illustrated in Figure 3. A small amount of additional time per MD timestep – averaging around 8 ms – was required to carry out the required calculations for the two-temperature model, i.e. calculations of ionic temperatures from atomic velocities and evolution of electronic temperatures. The effect that these additional calcu-

Table 1.: Results of strong scalability study for DL_POLY_4with and without the two-temperature model on Phase 2 of ARCHER.

Number of cores	Time per MD timestep/ms	
	TTM	No TTM
12	1075.1	1058.5
24	546.89	554.43
48	294.99	288.85
96	163.41	154.45
192	91.95	88.16
384	72.28	59.84
768	58.62	47.65
1536	51.23	40.80

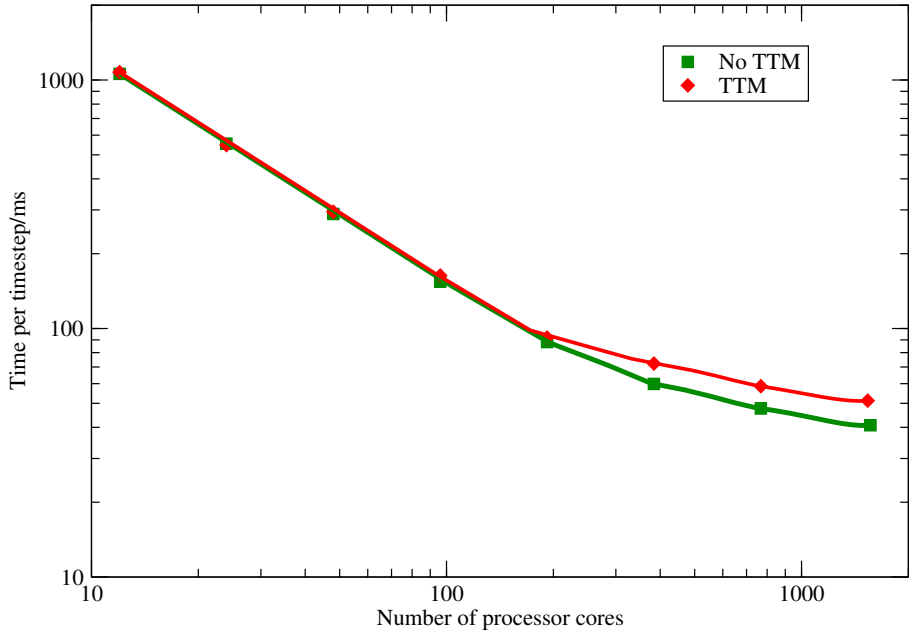

Figure 3.: Strong scaling of DL_POLY_4 with and without the two-temperature model on Phase 2 of ARCHER.

lations have on the parallel scalability is small, making the TTM calculations slightly less scalable when larger numbers of processor cores are used but not affecting the general trends. In both cases, the increase in computational speed with number of cores starts to level off at larger core counts, matching up well with expected behaviour for a domain-decomposed parallel MD code. The chosen strategy of dividing the temperature grids among the processor cores, using core-to-core communication between them, does not appear to significantly affect the overall parallel scalability or performance of DL_POLY_4 and is thus suited for larger scale simulations.

5. Applications of TTM with DL_POLY

A number of simulations have been carried out with modified versions of DL_POLY_3 and DL_POLY_4 that have incorporated the above-mentioned TTM functionalities [13]. These can be divided between radiation damage cascades, laser irradiation and swift heavy ion (SHI) irradiation.

5.1. *Cascades*

The original TTM developments for DL_POLY were intended for radiation damage simulations modelled using cascades. Domain-decomposed versions of DL_POLY (DL_POLY_3 and DL_POLY_4) include the capability to produce specialised output files recording defects (interstitials and vacancies) compared to a given initial structure at user-defined intervals [10], reducing the amounts of data written to a file for cascade simulations compared with full trajectory data.

The first 2T-MD studies with DL_POLY [6, 7] applied modifications to DL_POLY_3, making use of a replicated-data strategy for populating and evolving the ionic and electronic temperature grids. The simplicity of this method is countered by its requirements for global communications among all processor cores to populate the grids and for all cores to apply FDM calculations over the entire electronic temperature grid, restricting the parallel scalability of the TTM calculations. System sizes were consequently limited to around 250 000 atoms and energies of tens of kiloelectronvolts, but these first studies demonstrated the usefulness of 2T-MD in determining realistic extents of damage for materials with enhanced electron-phonon coupling.

The changes made to DL_POLY_3 were later included with DL_POLY_4 [19] and subsequently re-engineered as detailed above to parallelise the temperature grids in a similar fashion to the main body of the MD code. The first cascade-based applications making use of DL_POLY_4 with domain-decomposed TTM examined radiation damage cascades of 100–500 keV in up to 150 million atoms of α-iron [17], zirconia [20] and tungsten [21]. The simulations modelling these cascades were carried out on the UK national supercomputer at the time, HECToR Phase 3, using up to 65 536 cores (nearly three-quarters) of this machine.

An example of the radiation damage observed during these simulations can be found in Figure 4. Comparisons were made of α-iron calculations using the inhomogeneous Langevin thermostat for electronic stopping only [22] against those with the full TTM implementation: these demonstrated that including energy transfers between atomistic and electronic systems resulted in fewer displacements and defects at the peak level of damage and subsequently more rapid recovery.

Further cascade studies based on 2T-MD using DL_POLY_4 have been carried out for nickel-based systems [23, 24], including alloys of nickel with iron or palladium [25–27], using up to 20 million atoms and energy impacts of up to 150 keV. The inclusion of electron-phonon and electronic stopping effects in these simulations produces more realistic extents of damage than other modelling methods, as well as demonstrating that, for a given impact, the alloys are damaged less than pure nickel.

5.2. *Laser irradiation*

The first 2T-MD simulations of laser irradiation with DL_POLY_4 examined systems with gold nanofilms [28, 29], using spatially Gaussian and temporally exponential energy depositions to the electronic temperature grid to represent the excitation fluences. While corresponding DFT calculations indicate that the atomistic potential changes at higher electronic temperatures (above 9000K), the ground-state potential is still sufficient to accurately reproduce e.g. Bragg peak evolution and melting processes for lower energy fluences.

Further laser irradiation simulations using DL_POLY_4's 2T-MD implementation have been carried out for thin films of tungsten [16, 30], albeit making modifications to the code to incorporate

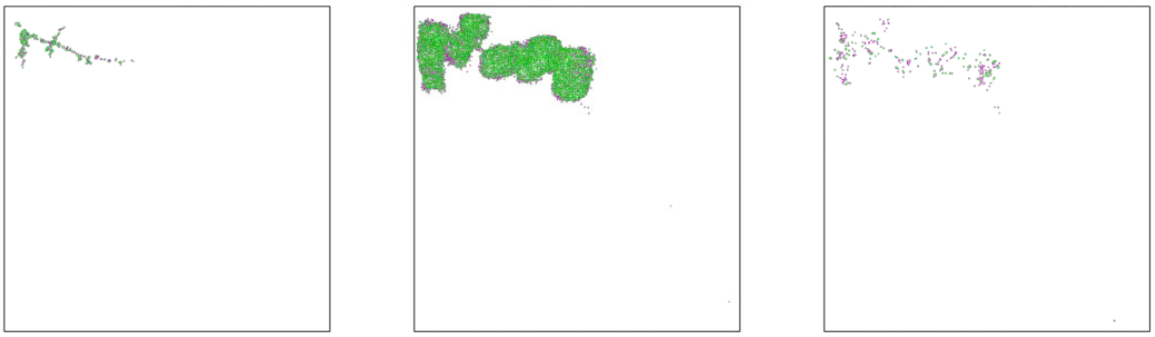

(a) (b) (c)

Figure 4.: A representative 200 keV cascade in 100 million atoms of α-iron modelled using DL_POLY_4 with TTM, showing defect atoms from the original structure with vacancies (interstitials) shown in purple (green): the processes resulting from the cascade include (a) fracturing, (b) annealing and (c) healing of the metallic structure. (Images based on work carried out in [17], courtesy of Eva Zarkadoula.)

embedded atom model (EAM) potentials that depend on local electronic temperature. The latter were needed for higher energy fluences (up to 80 mJ cm^{-2}), as maximum electronic temperatures of approximately 22 000K were reached. The simulations were able to examine the dynamics of ultrafast solid-solid phase transformations, as well as demonstrate the expansion of thin films due to electronic excitation.

5.3. *Swift heavy ion irradiation*

Simulations examining the response of germanium to swift heavy ion (SHI) radiation [31] were the first calculations of this kind to be carried out using DL_POLY_4 with the additional TTM functionality. In this case, the TTM was extended by including an additional conservation equation for the electron density [32], which is also evolved using a finite-difference method and used as a parameter in place of the electronic specific heat (C_e) in Equation (4). Using an atomistic system of 200 000 germanium atoms and an electronic temperature grid expanded outwards orthogonally to the direction of energy deposition, the effect of electronic stopping power on amorphised latent track radii could be determined. These simulations were able to realistically account for non-equilibrium carrier dynamics in an irradiated band gap material, providing good agreement with experimental data on track radii.

Simulations of SHI radiation on silicon with 2T-MD [33] further demonstrated the usefulness of this method in studying band gap materials (insulators and semiconductors). As an alternative to evolving electron densities, this work included determination of the electronic specific heat of silicon as a function of electronic temperature using DFT calculations. Determination of specific heats allowed proper parameterisation of the two-temperature model's heat diffusion part and tabulated values could be included as an input for DL_POLY_4. Similar calculations for body-centred (iron and tungsten) and face-centred (copper and nickel) cubic metals, modelling around 2.4 million atoms of each, also made use of DFT calculations to determine electron-phonon coupling coefficients (g_p) as functions of electronic temperature [34]. These simulations demonstrated the sensitivity of electron-phonon coupling to the extent and type of damage: the body-centred cubic metals were more resistant, while elongated dislocation loops in the direction of the ion path were formed in face-centred metals.

6. Summary and outlook

The implementation of the two-temperature model in DL_POLY_4 significantly widens the range of simulations possible with this molecular dynamics code to include systems where excitation of electrons plays an important role. Applying domain decomposition to the temperature grids in a similar manner to the atomistic system ensures the parallel scalability of TTM-based calculations alongside atomistic MD, allowing systems with many millions of atoms to be modelled efficiently with radiation damage cascades, laser depositions and swift heavy ion irradiation. Several 2T-MD (TTM/MD-coupled) systems have already been simulated using DL_POLY_4, providing greater insight into the effects of radiation damage and irradiation on various solid structures and indications of future TTM-related development (e.g. T_e-dependent atomistic potentials) in this code.

The next release of DL_POLY_4 (version 4.09) will make TTM available to all code users along with several ancillary features to enable simulations of a wide range of materials with explicit electronic stopping and electron-phonon coupling. The user manual will be updated to include details of the TTM implementation in DL_POLY_4, and three new demonstration simulations – representing systems with cascades, laser depositions and swift heavy ion irradiation – will be included in the code's test suite. The code will be made available from the DL_POLY_4 website (www.ccp5.ac.uk/DL_POLY).

Acknowledgements

Funding by EPSRC (EP/I029354/1) for the code development work outlined in this article is gratefully acknowledged. MAS and ITT would also like to thank Kostya Trachenko (Queen Mary University of London) for instigating the fruitful collaboration leading to this work, Eva Zarkadoula (now at Oak Ridge National Laboratory) for extensive beta testing of DL_POLY_4 with the domain-decomposed two-temperature model and Samuel Murphy (Lancaster University) for prototyping T_e-dependent potentials with this code.

References

[1] Malerba L. Molecular dynamics simulation of displacement cascades in α-fe: A critical review. Journal of Nuclear Materials. 2006;351:28–38; proceedings of the Symposium on Microstructural Processes in Irradiated Materials; Available from: http://www.sciencedirect.com/science/article/pii/S0022311506000638.

[2] Stoller R. Primary radiation damage formation. In: Konings RJ, editor. Comprehensive nuclear materials. Oxford: Elsevier; 2012. p. 293–332; Available from: https://www.sciencedirect.com/science/article/pii/B9780080560335000276.

[3] Flynn CP, Averback RS. Electron-phonon interactions in energetic displacement cascades. Physical Review B. 1988 Oct;38:7118–7120; Available from: https://link.aps.org/doi/10.1103/PhysRevB.38.7118.

[4] Stoneham A. Energy transfer between electrons and ions in collision cascades in solids. Nuclear Instruments and Methods in Physics Research Section B: Beam Interactions with Materials and Atoms. 1990; 48:389–398; Available from: http://www.sciencedirect.com/science/article/pii/0168583X9090147M.

[5] Caro A, Victoria M. Ion-electron interaction in molecular-dynamics cascades. Physical Review A. 1989 Sep;40:2287–2291; Available from: https://link.aps.org/doi/10.1103/PhysRevA.40.2287.

[6] Duffy DM, Rutherford AM. Including the effects of electronic stopping and electron–ion interactions in radiation damage simulations. Journal of Physics: Condensed Matter. 2007;19:016207; Available from: http://stacks.iop.org/0953-8984/19/i=1/a=016207.

[7] Rutherford AM, Duffy DM. The effect of electron–ion interactions on radiation damage simulations. Journal of Physics: Condensed Matter. 2007;19:496201; Available from: http://stacks.iop.org/0953-8984/19/i=49/a=496201.

[8] Pinches MRS, Tildesley DJ, Smith W. Large scale molecular dynamics on parallel computers using the link-cell algorithm. Molecular Simulation. 1991;6:51–87; Available from: https://doi.org/10.1080/08927029108022139.
[9] Todorov IT, Smith W. DL_POLY_3: the CCP5 national UK code for molecular-dynamics simulations. Philosophical Transactions of the Royal Society of London A. 2004;362:1835–1852; Available from: http://rsta.royalsocietypublishing.org/content/362/1822/1835.abstract.
[10] Todorov IT, Smith W, Trachenko K, et al. DL_POLY_3: new dimensions in molecular dynamics simulations via massive parallelism. Journal of Materials Chemistry. 2006;16:1911–1918.
[11] Plimpton S. Fast parallel algorithms for short-range molecular dynamics. Journal of Computational Physics. 1995;117:1–19; Available from: http://www.sciencedirect.com/science/article/pii/S002199918571039X.
[12] Crank J. The mathematics of diffusion. 2nd ed. Oxford: Clarendon Press; 1975.
[13] Darkins R, Duffy DM. Modelling radiation effects in solids with two-temperature molecular dynamics. Computational Materials Science. 2018;147:145–153; Available from: https://www.sciencedirect.com/science/article/pii/S0927025618300892.
[14] Seaton M, Anderson R, Metz S, et al. DL_MESO: highly scalable mesoscale simulations. Molecular Simulation. 2013;39:796–821.
[15] Norman GE, Starikov SV, Stegailov VV. Atomistic simulation of laser ablation of gold: effect of pressure relaxation. Journal of Experimental and Theoretical Physics. 2012 May;114:792–800; Available from: https://doi.org/10.1134/S1063776112040115.
[16] Murphy ST, Daraszewicz SL, Giret Y, et al. Dynamical simulations of an electronically induced solid-solid phase transformation in tungsten. Physical Review B. 2015 Oct;92:134110; Available from: https://link.aps.org/doi/10.1103/PhysRevB.92.134110.
[17] Zarkadoula E, Daraszewicz SL, Duffy DM, et al. Electronic effects in high-energy radiation damage in iron. Journal of Physics: Condensed Matter. 2014;26:085401; Available from: http://stacks.iop.org/0953-8984/26/i=8/a=085401.
[18] Malerba L, Marinica M, Anento N, et al. Comparison of empirical interatomic potentials for iron applied to radiation damage studies. Journal of Nuclear Materials. 2010;406:19–38; fP6 IP PERFECT Project: Prediction of Irradiation Damage Effects in Reactor Components; Available from: http://www.sciencedirect.com/science/article/pii/S0022311510002291.
[19] Daraszewicz S. The modelling of electronic effects in molecular dynamics simulations EngD thesis. Department of Physics and Astronomy & London Centre for Nanotechnology, University College London; 2013.
[20] Zarkadoula E, Devanathan R, Weber WJ, et al. High-energy radiation damage in zirconia: modeling results. Journal of Applied Physics. 2014 Feb;115:083507; Available from: http://scitation.aip.org/content/aip/journal/jap/115/8/10.1063/1.4866989.
[21] Zarkadoula E, Duffy DM, Nordlund K, et al. Electronic effects in high-energy radiation damage in tungsten. Journal of Physics: Condensed Matter. 2015;27:135401; Available from: http://stacks.iop.org/0953-8984/27/i=13/a=135401.
[22] Zarkadoula E, Daraszewicz SL, Duffy DM, et al. The nature of high-energy radiation damage in iron. Journal of Physics: Condensed Matter. 2013;252:125402; Available from: http://stacks.iop.org/0953-8984/25/i=12/a=125402.
[23] Zarkadoula E, Samolyuk G, Xue H, et al. Effects of two-temperature model on cascade evolution in Ni and NiFe. Scripta Materialia. 2016;124:6–10; Available from: http://www.sciencedirect.com/science/article/pii/S1359646216302822.
[24] Zarkadoula E, Samolyuk G, Weber WJ. Effects of electronic excitation in 150 keV Ni ion irradiation of metallic systems. AIP Advances. 2018;8:015121; Available from: https://doi.org/10.1063/1.5016536.
[25] Zarkadoula E, Samolyuk G, Weber WJ. Two-temperature model in molecular dynamics simulations of cascades in Ni-based alloys. Journal of Alloys and Compounds. 2017;700:106–112; Available from: http://www.sciencedirect.com/science/article/pii/S0925838816343705.
[26] Zarkadoula E, Samolyuk G, Weber WJ. Effects of the electron-phonon coupling activation in collision cascades. Journal of Nuclear Materials. 2017;490:317–322; Available from: http://www.sciencedirect.com/science/article/pii/S0022311517301216.
[27] Zarkadoula E, Samolyuk G, Weber WJ. Effects of electronic excitation on cascade dynamics in nickel–iron and nickel–palladium systems. Scripta Materialia. 2017;138:124–129; Available from:

http://www.sciencedirect.com/science/article/pii/S1359646217302932.

[28] Giret Y, Naruse N, Daraszewicz SL, et al. Determination of transient atomic structure of laser-excited materials from time-resolved diffraction data. Applied Physics Letters. 2013;103:253107; Available from: http://scitation.aip.org/content/aip/journal/apl/103/25/10.1063/1.4847695.

[29] Daraszewicz SL, Giret Y, Naruse N, et al. Structural dynamics of laser-irradiated gold nanofilms. Physical Review B. 2013 Nov;88:184101; Available from: http://link.aps.org/doi/10.1103/PhysRevB.88.184101.

[30] Murphy ST, Giret Y, Daraszewicz SL, et al. Contribution of electronic excitation to the structural evolution of ultrafast laser-irradiated tungsten nanofilms. Physical Review B. 2016 Mar;93:104105; Available from: https://link.aps.org/doi/10.1103/PhysRevB.93.104105.

[31] Daraszewicz S, Duffy D. Hybrid continuum–atomistic modelling of swift heavy ion radiation damage in germanium. Nuclear Instruments and Methods in Physics Research Section B: Beam Interactions with Materials and Atoms. 2013;303:112–115; proceedings of the 11th Computer Simulation of Radiation Effects in Solids (COSIRES) Conference Santa Fe, New Mexico, USA, July 24-29, 2012; Available from: http://www.sciencedirect.com/science/article/pii/S0168583X12007690.

[32] van Driel HM. Kinetics of high-density plasmas generated in Si by 1.06- and 0.53-μm picosecond laser pulses. Physical Review B. 1987 May;35:8166–8176; Available from: https://link.aps.org/doi/10.1103/PhysRevB.35.8166.

[33] Khara GS, Murphy ST, Daraszewicz SL, et al. The influence of the electronic specific heat on swift heavy ion irradiation simulations of silicon. Journal of Physics: Condensed Matter. 2016;28:395201; Available from: http://stacks.iop.org/0953-8984/28/i=39/a=395201.

[34] Khara GS, Murphy ST, Duffy DM. Dislocation loop formation by swift heavy ion irradiation of metals. Journal of Physics: Condensed Matter. 2017;29:285303; Available from: http://stacks.iop.org/0953-8984/29/i=28/a=285303.